"Learning from Deep Learning"
Lessons from using computer vision to identify (urban) form and function in open data satellite imagery

Martin Fleischmann[*†§]
Daniel Arribas-Bel[*†‡¶]

Geographic Data Science Lab, University of Liverpool
The Alan Turing Institute

ABSTRACT: The building blocks that make up cities -the activities and agents conceptualised as urban function, and the structure that supports them conceptualised as urban form- can be spatially arranged in many ways. This paper relies on the concept of "spatial signatures", a characterisation of space designed to understand urban environments, that exhaustively divide geographical space into distinct classes based on form and function. Due to the dependency on data sources that are being updated at a variable rate, signatures cannot be easily updated with frequency. One possible solution comes from remote sensing and satellite imagery. While staying in the realm of open data, we explore this pathway using the Sentinel-2 imagery within a deep convolutional neural network (CNN) trained to predict spatial signature type across Great Britain. Our focus is not only to develop a performant CNN but also to learn about the nature of the classes we try to predict (appropriate scale, inter-class relationships) through the lens provided by the neural network. With Sentinel-2 being relatively coarse in the resolution, there are not only technical questions of the CNN architecture, but also geographical ones related to the Modifiable Areal Unit Problem and the ability of samples to capture the nature of each signature type. Furthermore, there is the question of to which degree signatures can be seen from space. We present exploratory work and empirical experiments, and discuss the opportunities and challenges in using remote sensing to reliably detect concepts like spatial signatures using openly available satellite imagery.

Key words: spatial signatures, classification, remote sensing, artificial intelligence, open data

[*]THANKS.

[†]Geographic Data Science Lab, Department of Geography and Planning, University of Liverpool, Roxby Building , 74 Bedford St S , Liverpool , L69 7ZT, United Kingdom

[§]E-mail: M.Fleischmann@liverpool.ac.uk; website: https://martinfleischmann.net/.

[‡]E-mail: D.Arribas-Bel@liverpool.ac.uk; phone: +44 (0)151 795 9727; website: http://darribas.org.

[¶]The Alan Turing Institute, British Library, 96 Euston Road, London, England, NW1 2DB, United Kingdom

1. Introduction

2. Materials and Methods

In this section we present the materials used in the research - the British spatial signatures used as to generate labels for individual chips and Sentinel 2 satellite imagery - and methods designed to unpack the role of geography in image-based deep learning.

2.1 Materials

The whole research uses only two data inputs, one representing the "ground truth" we are aiming to predict using neural networks and the other representing the satellite imagery. While the latter does not need a lot of introduction, the British spatial signatures used as the labels need to be explained further.

2.1.1 British Spatial Signatures

Spatial signatures are a way of classification of space covering entirety of a case study area. They are defined as *"a characterisation of space based on form and function designed to understand urban environments"* (Arribas-Bel and Fleischmann, 2022) and the definition already points at the clear distinction between signatures and traditional Land Use / Land Cover (LULC) classifications. Taking the example of CORINE (European Environment Agency, 1990) as a representative of LULC, it has 44 distinct classes, out of which 2 cover urban form and other 6 can be loosely related to urban areas[1]. A similar situation is with recently released global LULC datasets. European Space Agency's WorldCover project distinguishes 11 classes of which one is urban (Built-up) (Zanaga et al., 2021). Esri's Land cover has 9 classes where one is *Built Area* and the rest covers unbuilt areas (Karra et al., 2021). This ratio of built vs unbuilt classes is typical but not very suited for research applications focusing on urban environments. Spatial signatures tend to flip this ratio as they are primarily classifying urban space.

There are two key main concepts embedded in spatial signatures delivering urban-focused classification. The first one is the spatial unit called the enclosed tessellation cell (ETC). To derive ETCs, we first generate *enclosures*, a space fully enclosed by a set of barriers (roads, railways, rivers, coastline). ETCs are then a result of Voronoi tessellation based on building footprint polygons. The resulting spatial unit has adaptive granularity reflecting the scale of each individual urban pattern. The second is the selection of characters describing each ETC. We measure form and function, both primarily urban phenomena and mostly omit environmental aspects focusing on land cover patterns.

British spatial signatures as presented in Fleischmann and Arribas-Bel (2022) are one application of the concept of spatial signatures in the context of Great Britain. It divides the space into 16 data-driven classes (Figure 1) listed in Table 1. Out of these 16 classes, nine are entirely urban, four are peripheral and only three are classifying natural spaces, inverting the ratio of built vs

---

[1]Continuous urban fabric, Discontinuous urban fabric; Construction sites, Green urban areas, Sport and leisure facilities, Industrial or commercial units, Road and rail networks and associated land, Port areas

Signature type	area (sq.km)	ETC count	area (%)	ETCs (%)
Countryside agriculture	93,856.1	3,022,385	41	21
Accessible suburbia	2,244.5	1,962,830	1	14
Dense residential neighbourhoods	957.2	502,835	0	3
Connected residential neighbourhoods	565.4	374,090	0	3
Dense urban neighbourhoods	570.6	238,639	0	2
Open sprawl	5,081.5	2,561,211	2	18
Wild countryside	91,306.3	595,902	40	4
Warehouse/Park land	2,462.4	707,211	1	5
Gridded residential quarters	261.2	209,959	0	1
Urban buffer	31,588.8	3,686,554	14	25
Disconnected suburbia	708.9	564,318	0	4
Local urbanity	231.1	86,380	0	1
Concentrated urbanity	7.8	1,390	0	0
Regional urbanity	76.4	21,760	0	0
Metropolitan urbanity	16.5	3,739	0	0
Hyper concentrated urbanity	2.2	264	0	0

Table 1: Classes of British spatial signatures and their coverage in terms of area and a number of ETCs.

unbuilt classes known from LULC. However, out of these 16 classes, some are very rare and it would not be feasible to attempt to predict them. Therefore, we merge five classes falling under the "urbanity" group into a single one and use resulting 12 classes throughout this paper.

2.1.2 Sentinel 2 imagery

The second data input used in this research is satellite imagery provided by the Sentinel 2 mission. Specifically, we use the pre-processed cloud-free mosaic of Sentinel 2 released by Corbane et al. (2020). The mosaic provides pixel-level composite based on imagery for the period January 2017-December 2018 at an original resolution of 10 meters per pixel. While Sentinel 2 captures many spectral bands beyond traditional visible red, green and blue (RGB), this research uses only RGB bands due to its employment of pre-trained neural networks stemming from non-satellite imagery that is composed only of RGB. The exclusion of other bands may be seen as a limiting factor of the work, but we believe that, as with other aspects that will be discussed later, it efficiently illustrates the *lower bound* of the performance of presented method and can be only improved with addition of further spectral bands or other data (e.g. synthetic-aperture radar imagery).

Another notable aspect of the Sentinel 2 imagery is the resolution. Ten meters per pixel may be enough to distinguish LULC classes as shown by the research project discussed above. However, there is the question of whether it is enough to segment urban environments. Individual buildings often do not stretch beyond the spatial extent of two pixels, which is severely limiting what we can *see* on the image, as illustrated in Figure 1. While other data sources may provide better
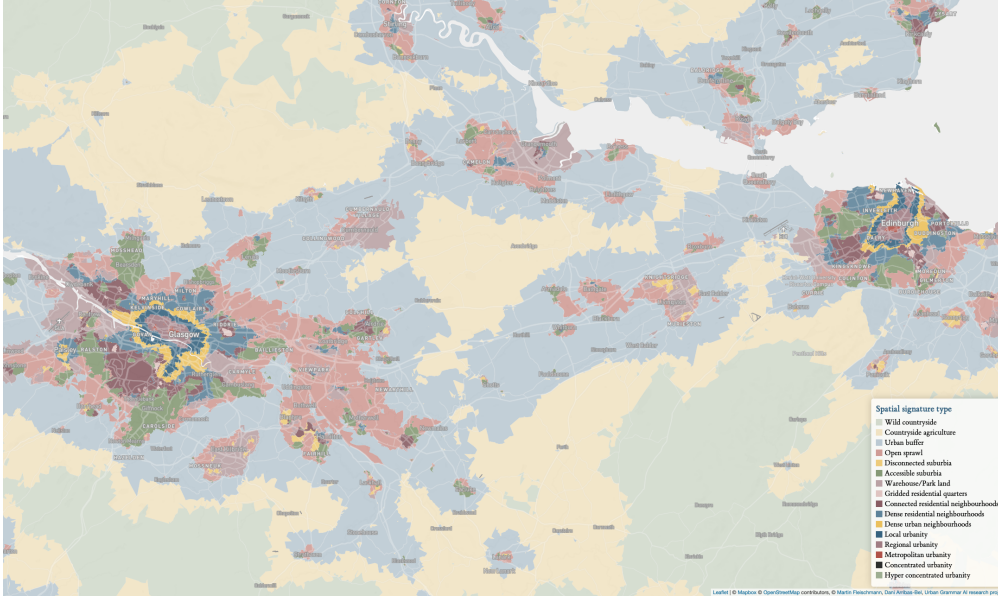
Figure 1: Spatial signatures in the area of the Scottish Central Belt stretching from Glasgow to Edinburgh.

resolution[2], potentially improving model performance, this research is bound within the limits of *open data*, where Sentinel 2 is the best offering to date.

2.2 *Methods*

We define our challenge as an image classification task and use competing alternatives to explore which one performs best. Each of them imply geographically relevant trade-offs. First, we build and train a model composed of a convolutional neural network and probability modelling able to predict the 12 classes derived from the spatial signatures. Second, we use methods designed to unveil which of the inherently geographical decisions that are being tested has significant effect on the resulting performance and should therefore be taken into account when applying CNN on spatial problems.

Overall, our exercise is structured as a comparison of models that attempt to predict the 12 spatial signatures entirely from Sentinel 2 imagery. Each model takes a set of chips as input, runs the class prediction using the convolutional neural network (CNN) and builds a (spatial) model on top of the resulting probabilities. The differences between the models are capturing the geographical options being tested - an extent of the area sampled from the satellite imagery into a single *chip*, presence of spatial augmentation, class exclusivity within each chip, and an architecture of probability modelling on top a prediction coming from the CNN.

Finally, performance of each model is assessed using both traditional non-spatial techniques used in deep learning and bespoke spatial metrics. Given the large number of resulting values, a regression approach is used to determine the effect of the tested options.

Each of the steps is further discussed in detail in the subsequent sections.

---

[2]For example, commercial imagery by Maxar reaches a resolution of 30cm per pixel and imagery by Planet of 50cm per pixel

2.2.1 Chip size

The first question that needs to be answered when trying to apply a classification algorithm on satellite imagery that span a large amount of continuous land is how to sample such data into individual patches (or, hereafter, chips) that can be assigned to classes. Pre-trained CNNs usually expect a square image of certain size but that does not mean that the same size (in terms of pixels) needs to be directly sampled from the image thanks to possible resampling. What should be retained though, is the ratio. Therefore, we need to sample square chips of custom size. Within an image classification framework, we assume that each chip contains data of a single class only. Therefore, such a chip should be fully within the boundary of a single signature type. That poses some restrictions as spatial signatures, especially in urban context, tend to be relatively granular and large chips would simply not fit inside the boundaries, therefore reducing the amount of valid chips for training. The goal is therefore to find a balance between the number of chips that can be sampled from the data and an amount of information each chip can hold. Given the relatively coarse resolution of Sentinel 2, a chip of 100x100 meters consists of only 10x10 pixels, which may not be enough to capture the nature of a signature type and distinguish it from other types. On the other hand, a chip of 1000x1000 meters, that is likely large enough to capture the difference, will not fit in most of the signature boundaries and we would end with only a few chips per urban class.

The literature rarely discusses this decision-making process when defining the chip size. In some cases, the size is predetermined due to the requirement of either a pre-trained model or existing set of labelled data (Taubenböck et al., 2020). In other ones, the size that has been used in previous studies is applied again without discussing the implications of such a decision (Wang et al., 2018). From a spatial analysis perspective, this approach is surprising as deciding the chip size is a prime example of the modifiable areal unit problem (also known as MAUP, Openshaw, 1981), especially the aspect about scale, which states that a change of the scale may affect the outcome of an experiment. Hence such an effect should be at least considered in an interpretation if not intentionally minimized.

In this work we try to understand the effect of a chip size by testing all the models based on four different chip sizes - 80, 160, 320 and 640 meters representing chips of 8x8, 16x16, 32x32 and 64x64 pixels, respectively, illustrated on a Figure 1.

2.2.2 (Spatial) data augmentation - Sliding

As mentioned above, certain chip sizes, in combination with the signature geometry and the requirement to keep them exclusively within a single class may result in an insufficient amount of training data for some signature types. Under-sampling like this one can be a serious problem, that is not unique to spatial modelling. However, traditional augmentation methods are not directly applicable here. For example, in an image classification problem trying to determine if there is a cat or a dog on an image, we can flip the picture along y axis, add some rotation or zoom to get more versions of the same image and expand the set of training data. Neither of these methods is applicable to spatial problems. Flipping or rotating the image would break natural
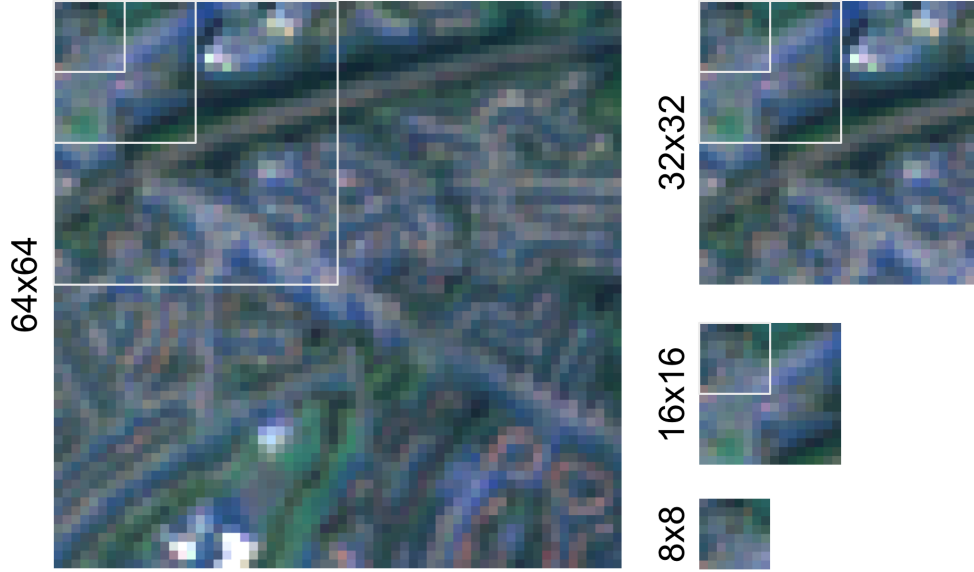
Figure 2: Illustration of the selected chip sizes using the Sentinel 2 cloud-free mosaic. Each of the chips also shows the sizes of the smaller options as a white outline.

light conditions, while zooming in would change the scale of urban environment we attempt to capture.

At the same time, the geographical and continuous nature of the data at hand allows us to use explicitly spatial augmentation techniques such as the one we call *sliding*. Sliding can be seen as overlapping sampling. Instead of overlaying a grid of chips over target geometry and using each pixel only once, we take the initial grid and slide it a few pixels horizontally and vertically as illustrated on a Figure 3. If the boundary of a slid chip is fully within a signature geometry, it is added to the pool of chips to be used. This process is done repeatedly to ensure that each class has a reasonable amount of chips to work with.

It is to be noted that sliding can cause a data leakage (sequences of pixels being present in both training and validation) if done before splitting the data into training and validation subsets. Therefore, we first create the initial grid, subdivide it spatially into four parts (40% for CNN training, 10% for CNN validation, 40% for probability modelling training, 10% for probability modelling validation) and apply sliding within each part to avoid any pixels being shared among chips from different sets.

2.2.3 *Model architecture*

Model architecture refers to the analytical pipeline that transforms chips into a prediction for a single signature type. Our competing architectures contain two main parts. First is a CNN that transforms a single chip into a set of 12 probabilities, one for each signature type. Second is a mathematical function that converts such probabilities (either considering only those for the chip of interest, or in conjunction with those of neighboring chips) into a prediction for a single signature type. This section describes each of these in detail. We would like to highlight that, contrary to the majority of deep learning-focused research, our focus is not on the architecture
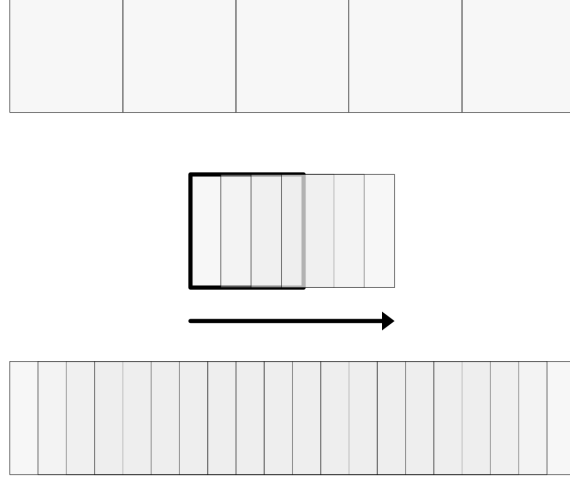
Figure 3: Diagram illustrating the sliding mechanism in one direction. The first row shows the initial non-overlapping grid, the last one final overlapping set of chips. The same approach is then also applied vertically.

of the CNN itself. We assume the effect of geographic choices will largely show similar behavior irrespective of the network architecture. For that reason, throughout our experiments we use `EfficientNetB4` (Tan and Le, 2019), pre-trained on the popular ImageNet dataset (Deng et al., 2009). Appendix A. shows a brief comparison of several standard neural network architectures and their performance on a subset of data to motivate our decision. We then apply transfer learning by re-training the top-layer of the pre-trained model and replacing it by a custom sequence of dense layers described below.

We consider three variants of the CNN. The default approach (which we will refer to `bic`, for "baseline image classification") is a standard image classification problem, using the sets of chips that are fully within a single signature types. The custom top layer of the pre-trained CNN then contains a Global Average Pooling (2D) layer, a dense layer with ReLu activation and 256 neurons, and a dense layer with the softmax activation and number of neurons equal to a number of classes (12). A result for a single chip is a collection of 12 probabilities of a chip belonging to each signature type. The sum of all probabilities is one. An extension of this approach (`sic`, for "sliding image classification) applies this technique to the data being spatially augmented with the sliding technique described above.

Our third approach recasts the image classification task as multiclass prediction. If we relax the requirement that every chip be fully within boundaries of a single signature type, we end up with many more available chips but now some of them include more than a single label within their extent. Instead of a single label per chip, we now deal with an array of them. This can be beneficial from the geographical perspective as such chips now inherently encode co-location of individual signature types and a model could use this information during the

prediction. As signature types usually tend to neighbor only a subset of other classes (e.g., Urbanity never neighbors Wild Countryside), we can assume that information on co-location can positively impact predictive performance. We then include a set of chips sampled from a grid crossing the boundaries of signature types (using the same chip sizes as before) and adapt the CNN to perform multi-output regression (mor) instead of image classification. This change implies the top layer is now composed of a Global Average Pooling (2D) layer a dense layer with ReLu activation and 256 neurons, and a dense layer with the sigmoid activation and a number of neurons equal to a number of classes (i.e., 12). The result for a single chip is a similar collection of probabilities, but these are now predicted proportions. As such, the sum of all of them ranges between 0 and 12, rather than between 0 and 1.

The second step in the pipeline takes chip probabilities and turns them into predictions of a signature type. To do this, we compare five approaches of differing complexity and sophistication. These five variants stem from the combination two components: the set of inputs used to make the prediction, and the function transforming them into a single signature type. For a given chip i, we can express this step of the pipeline mathematically as follows:

$$S_i = f(P)$$

$$P = \underbrace{\sum_k P_{k-i}}_{\text{baseline}} \underbrace{\left[+ \sum_k \sum_j w_{ij} P_{k-j} \right]}_{\text{wx}} \tag{1}$$

where S_i is the prediction for the signature type of chip i (one of the k available, where $k = 12$ in our case) and $f(\cdot)$ is a function that transforms the inputs P into S_i. The five approaches we compare derive from the different implementations of $f(\cdot)$ and P. On the latter, we compare models that only use the probabilities P_{k-i} generated by the CNN for chip i (baseline) with alternatives (signalled with the wx term) that, in addition, also include an average of P_{k-j} probabilities, which are the probabilities generated by the CNN for each neighbor j of chip i. This is akin to what in spatial analysis is called the *spatial lag* of each probability, and is calculated using a spatial weights matrix W that records the spatial relationship between every chip in the set. In our W, two neighboring locations i and j will receive a weight $w_{ij} = 1$, if they are in the same of the four split sets as defined above, and if they either are geographically contiguous or are nearest neighbors; while otherwise they will be consider non-neighbors and receive a weight $w_{ij} = 0$. To obtain an average of the neighbors, we row-standardise W so that $\sum_j w_{ij} = 1$. The second dimension other than P we vary is the function $f(\cdot)$ that converts it to the prediction S_i. We take three distinct approaches here: simply picking the maximum probability (maxprob), which we only use without the spatial lag of probabilities; an ensemble of binary logit models to predict each class (logite), then selecting the class with top probability, which we also use with the wx variant; and a histogram-based gradient boosted classifiers inspired by LightGMB (Ke et al., 2017) and implemented in scikit-learn (Pedregosa et al., 2011). This yields our five competing models: maxprob, logite_baseline, logite_baseline-wx, HGBC_baseline, and HGBC_baseline-wx.

2.2.4 Performance metrics

The goal of our experiments is to compare different models under varying geographical conditions to learn both which performs best, but also how different choices of geographical nature influence the overall performance when predicting form and function from satellite imagery. To provide a workbench that systematically compares each model and setup, we use a set of performance scores that operate either at the global or class level, and that measure performance in the traditional machine learning sense, as well as in the spatial sense.

We use four standard performance scores. *Cohen's kappa* score (κ, citealpcohen1960coefficient) is a measure of agreement between two sets of categorical labels that ranges from -1 to 1. Intuitively, it measures the extent to which the two sets agree with each other (i.e., same label for the same observation), beyond what would be expected from pure chance ($\kappa = 0$). Cases where there is more disagreement than expected from chance receive a negative score. *Global (within-class) accuracy* captures the proportion of observations correctly predicted (in a given class). The *Macro F1* is a score that aggregates class-based F1 scores. The F1 is the harmonic mean between precission (proportion of chips predicted in one class actually belonging to that class) and recall (proportion of chips belonging to a given class being predicted as such). We use both the *weighted Macro F1* as well as the *averaged Macro F1*. The latter takes the standard mean of the F1 scores for each class, while the former weights each F1 by the proportion of chips in each class.

In addition to traditional performance scores, we also evaluate how similar the spatial pattern of predictions is to that of the original labels. The measures described above are all "spatially unaware" in the sense that they quantify different aspects of the correctness of a model's predictions, but ignore their spatial patterning. Two sets of results may have the same amount of correct predictions, but in one the spatial layout of such predictions may be close to that of the observed labels, while the other one spatially allocates mispredictions in a way that differs more from what is observed empirically. Given the nature of our classification challenge –identify form and function over space from satellite imagery– the spatial dimension of model performance is of great importance. Since the spatial signatures represent a set of (12) distinct categories, we rely on the *join counts* statistic (JC, Cliff and Ord, 1981). The JC measures the degree of spatial concentration in a binary categorical variable; hence, we use it at the class level. For each class in each model, we retain the proportion of pairs of chips in the same class that are spatial neighbors ("joins") over the total number of pairs that are spatial neighbors. Our neighborhood definition relies on two alternative spatial weights matrices: one based on a distance threshold of $1Km$ (W_{thr}), and one that combines the nearest neighbor with those defined by contiguity (W_{union}). Our metric of interest is then the error (i.e., absolute value of the difference) between this proportion for the model of interest and that of the observed labels.

2.2.5 Summarizing experiments

The setup described above generates over 60 different models to be trained to predict 12 signature types, and six performance measures to evaluate them. Making sense of their results requires a

systematic approach that summarises them and provides explicit tests for the questions we are trying to answer. We achieve this goal by fitting linear regressions that explain performance scores for each model as a function of the characteristics of the setup evaluated. Specifically, we estimate the following two equations. First, for global scores, we run:

$$Perf_i = \alpha + \sum_m \delta_m M_i + \sum_a \gamma_a A_i + \beta_1 Chip\ Size_i + \beta_2 W_i + \epsilon_i \tag{2}$$

where $Perf_i$ is each of our four global performance scores measured for trained model in setup i; α is an intercept; M_i are indicator variables for the type of model we estimate (i.e., `maxprob`, `logite`, `HGBC`);[3] A_i are, similarly, indicator variables for the architecture used (i.e., `bic`, `sic`, `mor`);[4] $Chip\ Size_i$ captures the number of pixels the chips in the setup contain; W_s is another indicator variable that takes the value of one if the model includes the spatial lag of signature type probabilities and zero otherwise; and $\epsilon_i \sim \mathcal{N}(0, \sigma)$ is an i.i.d. error term.

Second, for class-based scores, we fit:

$$Perf_{i-s} = \alpha + \sum_m \delta_m M_i + \sum_a \gamma_a A_i + \beta_1 Chip\ Size_i + \beta_2 W_i + \beta_3 [\%]\ Obs_{i-s} + \sum_s \zeta_s S_{i-s} + \epsilon_{i-s} \tag{3}$$

where $[\%]\ Obs$ represents either the number of chips in signature s in setup i or as a proportion of the total; and S_{i-s} an indicator variable for the signature type s;[5] and the rest is as in Equation 2. Importantly for both equations, $\delta_m / \gamma_a / \beta_1 / \beta_2 / \beta_3 / \zeta_s$, parameters to be estimated by the regression model, provide a direct and formal test to the key questions we set out to answer with our experiments.

3. Results

Within-class accuracy by model can be seen in Figure 4 (a sister figure where scores are grouped by signature rather than by model can be found in Appendix B.). We can notice some consistent patterns already. The baseline image classification (`bic`) tends to underperform other architectures, especially on more urban signature types. On the other hand, mutli-output regression (`mor`) using the larger chip size (32 or 64) tends to show highest values across signature types and models. If we look at accuracy for individual signature types, both extremes (urbanity on one side and both countryside classes on the other) tend to be easiest to predict. Regarding models, there is no immediate conclusion to be made apart from a clear indication that the maximum probability (`maxprob`) approach is generally worse than any of the modelling, suggesting that there is a value in the modelling step. The within-class accuracy can be further explored using confusion matrices available as an Appendix C..

Whilst plotting accuracy is a way to build an intuition about the performance of individual options, it does not quantify their effects. The linear regressions shown in tables 2 and 3 provide

---

[3]We remove `HGBC` to avoid perfect collinearity and hence treat it as the reference model.

[4]We remove `BIC` to avoid perfect collinearity and hence treat it as the reference model.

[5]We remove `Accessible suburbia` to avoid perfect collinearity and hence treat it as the reference model.
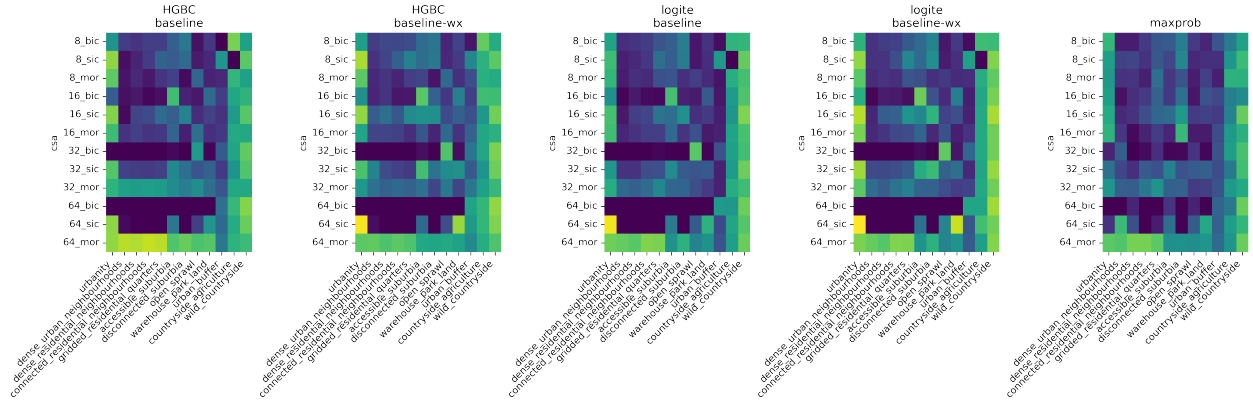
Figure 4: Within-class accuracy scores grouped by model. Each panel represents results from one of the five models compared, namely: histogram-based boosted classifier (`HGBC`) with features pertaining only to a given chip (`baseline`) or including also features from neighbouring ones (`baseline-wx`); Logit ensemble (`logite`) with the same two variations; and a simpler maximum probability approach (`maxprob`). Each row in the heatmap corresponds to a pair of chipsize (8, 16, 32, and 64 pixels) and architechture (baseline image classification, or `bic`; sliding image classification, or `sic`; and multi-output regression, or `mor`) used in the neural network stage of the pipeline. Colouring is standardised across panels and values range from 0 (dark purple) to 1 (bright yellow).

a better insight. The first regression explains global performance scores (Kappa, Global Accuracy, Marco F1 weighted and Macro F1 average). We can draw a few conclusions from this. First, there seems to be 0 positive effect of chip size on the results as it is consistently significant across all metrics. With the exception of average macro F1 score, there is a positive effect of inclusion of spatial lag in the modelling step (W). Regarding neural network step, we do not see a lot of significance but there are indications that sliding image classification and multi-output regression approaches outperform baseline image classification. Comparing the probability modelling step, we see an indication that the maximum probability is the least performant of the options, again suggesting the value of the modelling.

Table 3 then looks again at the within-class accuracy explaining what we have seen in the figure 4. We can see that multi-output regression consistently outperforms both baseline image classification and sliding image classification (which shows inconsistent results itself). Chip size has, again, a positive effect on the performance while the inclusion of spatial lag in the modelling is also consistently showing a positive impact. As assumed above, the prediction of signature types on both extremes of the urban-wild range tends to be easier than classes in between.

The regression outputs explaining differences in the spatial pattern between observed and predicted values, as measured by the Join Counts statistic offer another - spatially explicit - perspective on the performance of tested model configurations. As such it also indicates slightly different results as presented in a table 4 . Neither option of the probability modelling steps seem to have a significant effect on the Join Counts results unlike in previous performance metrics. However, the architecture of the neural network step shows significant effect as multi-output regression and in two out of four cases also sliding image classification outperform the baseline image classification. While the effect of chip size is inconsistent across the options, inclusion of spatial lag in the modelling step has significant effect (at either 10%, 5% or 1% significance level). The effect of a signature type depends on the their nature. More compact urban types

	κ	Global Accuracy	Macro F1 w.	Macro F1 avg.
Intercept	0.2185***	0.3236***	0.2790***	0.1798***
	(0.0209)	(0.0175)	(0.0174)	(0.0375)
(M) Logit E.	-0.0245	-0.0256*	-0.0324**	-0.0325
	(0.0168)	(0.0141)	(0.0141)	(0.0302)
(M) Max. Prob.	-0.0559**	-0.0606***	-0.0421**	-0.0296
	(0.0222)	(0.0187)	(0.0186)	(0.0399)
(A) M.O.R.	0.0227	-0.0357**	-0.0278*	0.1787***
	(0.0184)	(0.0155)	(0.0154)	(0.0331)
(A) S.I.C.	0.0232	-0.0247	-0.0171	0.1101***
	(0.0184)	(0.0155)	(0.0154)	(0.0331)
Chip Size	0.0036***	0.0043***	0.0048***	0.0014**
	(0.0004)	(0.0003)	(0.0003)	(0.0006)
W	0.0572***	0.0468***	0.0531***	0.0392
	(0.0168)	(0.0141)	(0.0141)	(0.0302)
R^2	0.7214	0.8281	0.8514	0.4191
R^2 Adj.	0.6899	0.8086	0.8346	0.3533
N.	60	60	60	60

Table 2: Regression outputs explaining global non-spatial performance scores. Explanatory variables with a preceding (M) and (A) correspond to binary variables for the type of model (with histogram-based boosted classifier, or HGBC, as the baseline) and architecture (with baseline image classification, or BIC, as the baseline), respectively. Standard errors in parenthesis. Coefficients significant at the 1%, 5%, 10% level are noted with ***, **, and *, respectively.

like *Urbanity* and *Dense urban neighbourhoods* show significance when using a distance threshold spatial weights, while sparser signature types like *Open Sprawl* and *Urban Buffer* show significance when using a union of weights.

4. Discussion

	Within-Class Accuracy		
Intercept	0.1866***	-0.0237	0.0595**
	(0.0308)	(0.0311)	(0.0303)
(M) Logit E.	-0.0125	-0.0125	-0.0125
	(0.0159)	(0.0141)	(0.0146)
(M) Max. Prob.	-0.0188	-0.0188	-0.0188
	(0.0211)	(0.0186)	(0.0193)
(A) M.O.R.	0.1753***	0.2512***	0.1753***
	(0.0175)	(0.0163)	(0.0160)
(A) S.I.C.	0.1202***	-0.0783***	0.1202***
	(0.0175)	(0.0209)	(0.0160)
Chip Size	0.0014***	0.0041***	0.0014***
	(0.0003)	(0.0003)	(0.0003)
1k Obs.		0.0514***	
		(0.0036)	
% Obs.			0.0156***
			(0.0013)
W	0.0365**	0.0365***	0.0365**
	(0.0159)	(0.0141)	(0.0146)
(S)Urbanity	0.2358***	0.2022***	0.2574***
	(0.0349)	(0.0309)	(0.0320)
(S)Dense urban neighbourhoods	-0.1420***	-0.1075***	-0.0998***
	(0.0349)	(0.0309)	(0.0322)
(S)Dense residential neighbourhoods	-0.1414***	-0.0836***	-0.0983***
	(0.0349)	(0.0311)	(0.0322)
(S)Connected residential neighbourhoods	-0.1306***	-0.0726**	-0.0754**
	(0.0349)	(0.0311)	(0.0323)
(S)Gridded residential quarters	-0.0785**	-0.0127	-0.0049
	(0.0349)	(0.0312)	(0.0326)
(S)Disconnected suburbia	-0.0601*	-0.0103	-0.0019
	(0.0349)	(0.0311)	(0.0324)
(S)Open sprawl	-0.0845**	-0.0995***	-0.1143***
	(0.0349)	(0.0309)	(0.0321)
(S)Warehouse park land	-0.0857**	-0.0788**	-0.0817**
	(0.0349)	(0.0309)	(0.0320)
(S)Urban buffer	-0.0828**	-0.1382***	-0.1753***
	(0.0349)	(0.0311)	(0.0330)
(S)Countryside agriculture	0.2236***	0.1593***	0.1118***
	(0.0349)	(0.0312)	(0.0334)
(S)Wild countryside	0.3876***	0.3283***	0.2925***
	(0.0349)	(0.0311)	(0.0330)
R^2	0.4979	0.6087	0.5794
R^2 Adj.	0.4857	0.5987	0.5686
N.	720	720	720

Table 3: Regression outputs explaining within-class accuracy. Explanatory variables with a preceding (M), (A) and (S) correspond to binary variables for the type of model (with histogram-based boosted classifier, or HGBC, as the baseline), architecture (with baseline image classification, or BIC, as the baseline) and spatial signature (with Accessible suburbia as the baseline), respectively. Standard errors in parenthesis. Coefficients significant at the 1%, 5%, 10% level are noted with ***, **, and *, respectively.

	JC W_thr	$\log(JC)$ W_thr	JC W_union	$\log(JC)$ W_union
Intercept	4.3454***	1.4617***	4.7103***	1.6311***
	(0.9507)	(0.1344)	(0.5763)	(0.1080)
(M) Logit E.	-0.1406	-0.0431	0.1851	0.0481
	(0.4951)	(0.0700)	(0.2995)	(0.0561)
(M) Max. Prob.	0.1128	-0.1223	0.2819	0.0223
	(0.6442)	(0.0911)	(0.3887)	(0.0728)
(A) M.O.R.	-3.1630***	-0.5744***	-2.7875***	-0.4647***
	(0.5494)	(0.0777)	(0.3301)	(0.0619)
(A) S.I.C.	0.0119	-0.2390***	-0.6666**	-0.0481
	(0.5532)	(0.0782)	(0.3329)	(0.0624)
Chip Size	0.0297***	-0.0005	-0.0061	-0.0080***
	(0.0108)	(0.0015)	(0.0065)	(0.0012)
W	-0.9325*	-0.1376**	-0.9556***	-0.1785***
	(0.4945)	(0.0699)	(0.2991)	(0.0560)
(S)Urbanity	4.6650***	0.6574***	0.1156	-0.1258
	(1.0696)	(0.1512)	(0.6460)	(0.1211)
(S)Dense urban neighbourhoods	1.7796*	0.5094***	0.7480	0.1609
	(1.0695)	(0.1512)	(0.6487)	(0.1216)
(S)Dense residential neighbourhoods	-0.8545	0.0672	-0.4636	-0.0920
	(1.0958)	(0.1550)	(0.6647)	(0.1246)
(S)Connected residential neighbourhoods	-0.3656	0.1543	-0.4388	-0.1447
	(1.1018)	(0.1558)	(0.6647)	(0.1246)
(S)Gridded residential quarters	-0.2000	0.1009	-0.6203	-0.2111*
	(1.0744)	(0.1519)	(0.6517)	(0.1221)
(S)Disconnected suburbia	-0.9752	-0.1719	-1.0303	-0.3358***
	(1.1213)	(0.1586)	(0.6684)	(0.1252)
(S)Open sprawl	1.8342*	0.1734	2.1575***	0.3576***
	(1.0604)	(0.1499)	(0.6432)	(0.1205)
(S)Warehouse park land	0.5496	0.2123	1.2245*	0.3054**
	(1.0694)	(0.1512)	(0.6487)	(0.1216)
(S)Urban buffer	-0.0558	-0.0931	2.7027***	0.5164***
	(1.0521)	(0.1488)	(0.6382)	(0.1196)
(S)Countryside agriculture	-1.3759	-0.2511*	0.6623	0.0670
	(1.0521)	(0.1488)	(0.6382)	(0.1196)
(S)Wild countryside	-2.0183*	-0.5065***	-0.5918	-0.1635
	(1.0521)	(0.1488)	(0.6382)	(0.1196)
R^2	0.1589	0.1954	0.2118	0.2660
R^2 Adj.	0.1368	0.1743	0.1913	0.2468
N.	665	665	670	670

Table 4: Regression outputs explaining (log of) differences in the spatial pattern between observed and predicted values, as measured by the Join Counts statistic. The Join Counts for each signature were computed using two types of spatial weights: one based on a distance threshold of 1Km (*W_thr*), and another one built as a the union of nearest neighbor and queen contiguity matrices (*W_union*). Explanatory variables with a preceding (M), (A) and (S) correspond to binary variables for the type of model (with histogram-based boosted classifier, or HGBC, as the baseline), architecture (with baseline image classification, or BIC, as the baseline) and spatial signature (with Accessible suburbia as the baseline), respectively. Standard errors in parenthesis. Coefficients significant at the 1%, 5%, 10% level are noted with ***, **, and *, respectively.

References

Arribas-Bel, D. and Fleischmann, M. (2022). Spatial Signatures - Understanding (urban) spaces through form and function. *Habitat International*, 0(0):0.

Cliff, A. D. and Ord, J. K. (1981). *Spatial processes: models & applications*. Taylor & Francis.

Corbane, C., Politis, P., Kempeneers, P., Simonetti, D., Soille, P., Burger, A., Pesaresi, M., Sabo, F., Syrris, V., and Kemper, T. (2020). A global cloud free pixel- based image composite from sentinel-2 data. *Data in Brief*, 31:105737.

Deng, J., Dong, W., Socher, R., Li, L.-J., Li, K., and Fei-Fei, L. (2009). Imagenet: A large-scale hierarchical image database. In *2009 IEEE conference on computer vision and pattern recognition*, pages 248–255. Ieee.

European Environment Agency (1990). CORINE Land Cover. pages 1–163.

Fleischmann, M. and Arribas-Bel, D. (2022). Geographical characterisation of british urban form and function using the spatial signatures framework. *Scientific Data*, 9(1):1–15.

Karra, K., Kontgis, C., Statman-Weil, Z., Mazzariello, J. C., Mathis, M., and Brumby, S. P. (2021). Global land use/land cover with sentinel 2 and deep learning. In *2021 IEEE international geoscience and remote sensing symposium IGARSS*, pages 4704–4707. IEEE.

Ke, G., Meng, Q., Finley, T., Wang, T., Chen, W., Ma, W., Ye, Q., and Liu, T.-Y. (2017). Lightgbm: A highly efficient gradient boosting decision tree. *Advances in neural information processing systems*, 30.

Openshaw, S. (1981). The modifiable areal unit problem. *Quantitative geography: A British view*, pages 60–69.

Pedregosa, F., Varoquaux, G., Gramfort, A., Michel, V., Thirion, B., Grisel, O., Blondel, M., Prettenhofer, P., Weiss, R., Dubourg, V., et al. (2011). Scikit-learn: Machine learning in python. *the Journal of machine Learning research*, 12:2825–2830.

Tan, M. and Le, Q. V. (2019). Efficientnet: Rethinking model scaling for convolutional neural networks.

Taubenböck, H., Debray, H., Qiu, C., Schmitt, M., Wang, Y., and Zhu, X. (2020). Seven city types representing morphologic configurations of cities across the globe. *Cities*, 105:102814.

Wang, R., Ren, C., Xu, Y., Lau, K. K.-L., and Shi, Y. (2018). Mapping the local climate zones of urban areas by gis-based and wudapt methods: A case study of hong kong. *Urban climate*, 24:567–576.

Zanaga, D., Van De Kerchove, R., De Keersmaecker, W., Souverijns, N., Brockmann, C., Quast, R., Wevers, J., Grosu, A., Paccini, A., Vergnaud, S., Cartus, O., Santoro, M., Fritz, S., Georgieva, I., Lesiv, M., Carter, S., Herold, M., Li, L., Tsendbazar, N.-E., Ramoino, F., and Arino, O. (2021). Esa worldcover 10 m 2020 v100.

Appendix A. Technical appendix

A. Comparison of neural network architechture

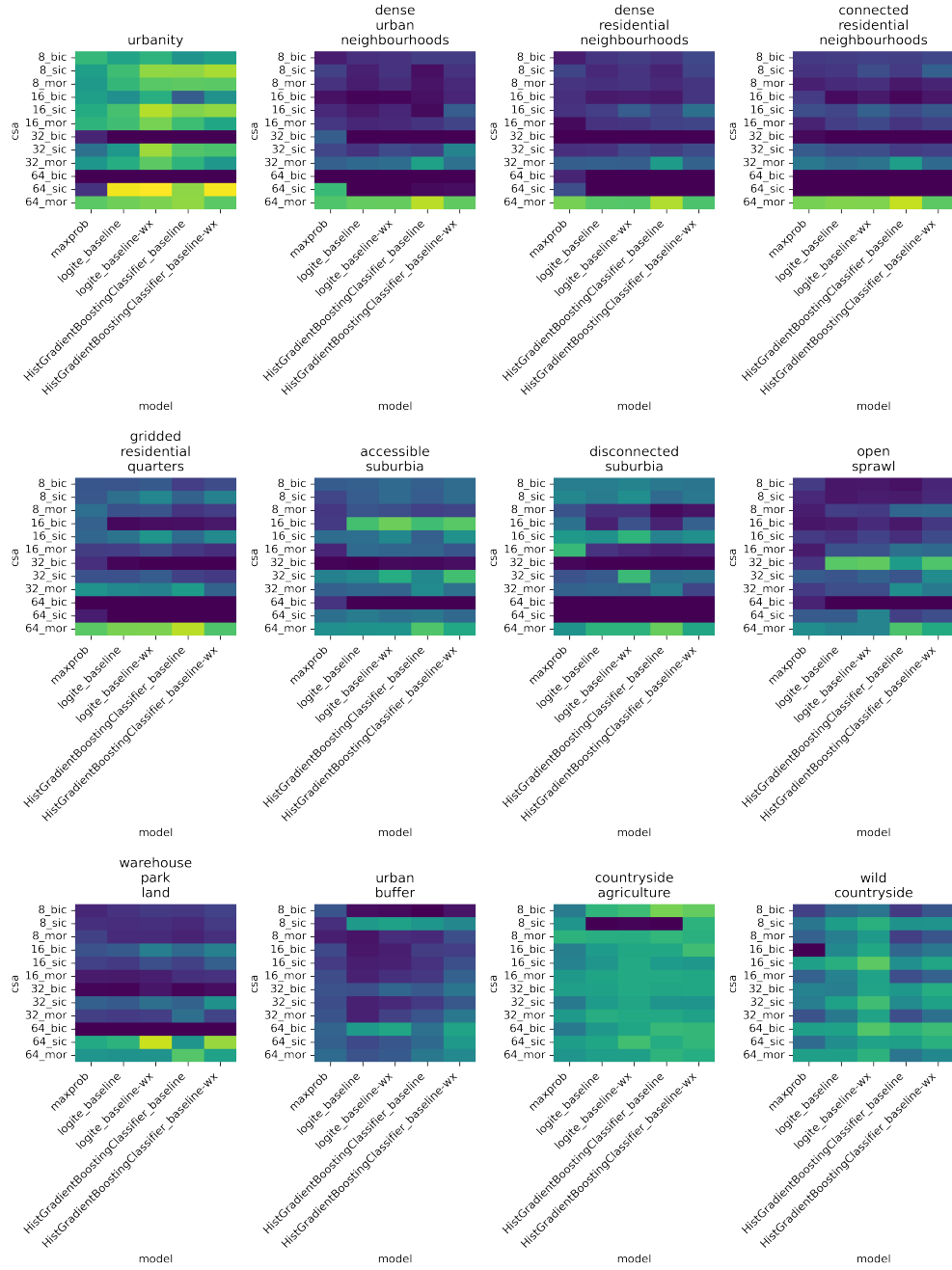*B. Within-class performance by spatial signature*

Figure 5: Within-class accuracy scores grouped by signature. Each panel represents results from one of the 12 signatures predicted. Each column in the heatmap corresponds to one of the five models compared, namely: histogram-based boosted classifier (HGBC) with features pertaining only to a given chip (baseline) or including also features from neighbouring ones (baseline-wx); Logit ensemble (logite) with the same two variations; and a simpler maximum probability approach (maxprob). Each row corresponds to a pair of chipsize (8, 16, 32, and 64 pixels) and architechture (baseline image classification, or bic; sliding image classification, or sic; and multi-output regression, or mor) used in the neural network stage of the pipeline.

C. Confusion matrices